Pseudospectral method for the Kardar-Parisi-Zhang equation

Lorenzo Giada*
International School for Advanced Studies (SISSA) and INFM Unità di Trieste, Via Beirut 2-4, Trieste I-34014, Italy

Achille Giacometti†
INFM Unità di Venezia, Dipartimento di Chimica Fisica, Università di Venezia, Calle Larga Santa Marta DD 2137, I-30123 Venezia, Italy

Maurice Rossi
Laboratoire de Modélisation en Mécanique, Université de Paris VI, 4 Place Jussieu, F-75252 Paris Cedex 05, France
(Received 11 December 2001; published 5 March 2002)

We discuss a numerical scheme to solve the continuum Kardar-Parisi-Zhang equation in generic spatial dimensions. It is based on a momentum-space discretization of the continuum equation and on a pseudospectral approximation of the nonlinear term. The method is tested in $(1+1)$ and $(2+1)$ dimensions, where it is shown to reproduce the current most reliable estimates of the critical exponents based on restricted solid-on-solid simulations. In particular, it allows the computations of various correlation and structure functions with high degree of numerical accuracy. Some deficiencies that are common to all previously used finite-difference schemes are pointed out and the usefulness of the present approach in this respect is discussed.

DOI: 10.1103/PhysRevE.65.036134 PACS number(s): 05.10.Gg, 81.15.−z, 68.55.−a

I. INTRODUCTION

Surface growth is a paradigmatic problem of nonequilibrium statistical mechanics with widespread potential applications such as molecular beam epitaxy, fluid flow in porous media or flame fronts [1,2].

For such extended systems, it is a rather intricate question how to connect, in a direct way, microscopic interactions to the dynamics at mesoscopic or coarse-grained scales. Phenomenological models, based on stochastic partial differential equations, selected according to symmetry principles and conservation laws, are often capable to reproduce various experimental data. The most well known of these models is the one introduced by Kardar, Parisi, and Zhang (KPZ) [3]. The equation introduced by these authors engendered an enormous amount of work that addressed the large number of issues related to it [4]. Yet, many fundamental properties of the KPZ equation are still not well understood. Using renormalization group (RG) theory, various authors attempted to estimate critical exponents and the upper critical dimension [5–8]. The success of this procedure has been limited, so far, by the difficulties of RG techniques to reach the strong-coupling regime. An alternative route to study stochastic partial differential equations, which yields an easy and reliable access to critical exponents, hinges on the so-called restricted solid-on-solid (RSOS) growth models [9–11]. This approach is based on simple rules for deposition and diffusion of particles on a discrete lattice, and it can be implemented in a very efficient and fast way on a computer. However, there is no *a priori* guarantee that a RSOS model belongs to the universality class of the continuum equation, albeit there is a general belief in this sense. Moreover, the corresponding coupling parameters possess fixed values in the RSOS case, a feature that prevents the exploration of the entire phase diagram of the KPZ equation.

Given these premises, numerical integration appears as the most direct and definite way to determine the universality class of a given continuum equation. So far, finite-differences methods have been exploited in the context of the KPZ equation [12–14]. In this framework, Lam and Shin [15] have shown the jeopardy of selecting an incorrect discretization in the framework of finite-differences algorithms. In this work, we follow a different route and propose a numerical scheme based on a pseudospectral representation.

Spectral methods, although almost routinely employed in fluid mechanics [16], have not, so far, been used in the context of stochastic equations except in Ref. [17]. In this latter work, two of us have introduced in the simple $(1+1)$ case, a discretization algorithm based on a pseudospectral scheme that outperforms classical finite differences on various respects. The present work generalizes the spectral method to the nontrivial $(2+1)$ case, where no exact results are available and where finite-differences methods may be hampered by large discretization effects, as we will shortly discuss. Extended numerical simulations for the $(2+1)$ case, are then reported, along with comparisons with results based on finite-differences schemes. The absence of uncontrolled discretization effects also allow us to compute various correlation functions and critical exponents in a rather precise and reliable way. Particularly interesting is the computation of various height-height correlation functions and of the structure factor, which were not previously calculated.

The plan of the remaining of the paper is as follows. In Sec. II, we address the general features of finite-differences discretizations and introduce the new pseudospectral procedure. Section III contains definitions of the various quantities

*Present address: MPIKG Golm, D-14424 Potsdam, Germany. Electronic address: giada@mpikg-golm.mpg.de

†Author to whom correspondence should be addressed. Electronic mail address: achille@unive.it

employed in this work as well as their pertinent scaling forms. Results are presented in Sec. IV for the $(1+1)$ dimensional and in Sec. V for the $(2+1)$-dimensional cases, respectively. Conclusions and perspectives are included in Sec. VI.

II. THE DISCRETIZED KPZ EQUATION

We consider a d-dimensional substrate and denote with $\mathbf{x}$ the d-dimensional vector locating a point on it. The surface, which grows on this substrate, is described at each time t by its height $h(\mathbf{x},t)$. In the continuum approximation, which disregards overhangs, this dynamics generically satisfies a stochastic partial differential equation

$$\partial_t h = \mathcal{F}(h) + \eta, \tag{1}$$

where $\mathcal{F}(h)$ is a functional containing various derivatives of $h(\mathbf{x},t)$, and $\eta(\mathbf{x},t)$ includes all the fluctuations produced by interactions among the unresolved microscopic degrees of freedom. This noise term clearly influences the dynamics at mesoscopic scales and, therefore, the global properties of these coarse-grained surfaces, in particular their rough or super-rough nature. In this work, we mainly focus on the case of white noise of zero average and amplitude D that is delta correlated in time as well as in space,

$$\langle \eta(\mathbf{x},t)\rangle = 0, \quad \langle \eta(\mathbf{x},t)\,\eta(\mathbf{x}',t')\rangle = 2D\,\delta^d(\mathbf{x}-\mathbf{x}')\,\delta(t-t'). \tag{2}$$

In Eq. (2) and below, the symbol $\langle\cdots\rangle$ represents ensemble averages over different realizations of the noise.

Constraints based on symmetry principles are helpful in reducing the functional $\mathcal{F}(h)$ to a few standard prescribed forms, according to the type of growth process it is expected to model. The KPZ equation [3], which is among the most common ones, reads

$$\partial_t h = \nu\nabla^2 h + \frac{\lambda}{2}(\nabla h)^2 + \eta, \tag{3}$$

where ν and λ denote coupling parameters for the linear and nonlinear terms, respectively. This equation contains, in addition to a linear diffusion term, a nonlinear term that takes into account the local growth normal to the interface [1,4]. In the following, fields are assumed to be periodic of characteristic length $L = V^{1/d}$ with respect to any spatial directions.

A. Finite-difference discretizations

In finite-differences methods, one discretizes space by defining points $\mathbf{x_j} = \mathbf{j}\Delta x$ ($\mathbf{j}$ being a set of d integer indices) on a cubic lattice of elementary size Δx. In the framework of a one step Euler time discretization, the KPZ time evolution reads

$$h(\mathbf{x_j}, t+\Delta t) = h(\mathbf{x_j},t) + \Delta t\left[\nu\nabla^2 h + \frac{\lambda}{2}(\nabla h)^2\right]_{\mathbf{x_j}} + \Delta t\,\eta(\mathbf{x_j},t), \tag{4}$$

where one sets

$$\eta(\mathbf{x_j},t) = \sqrt{\frac{24D}{(\Delta x)^d \Delta t}}\,\xi(\mathbf{j},t). \tag{5}$$

Here the factor ξ is a noise of zero average and correlation

$$\langle \xi(\mathbf{j},t)\,\xi(\mathbf{j}',t')\rangle = 2\,\delta_{\mathbf{j},\mathbf{j}'}\,\delta_{t,t'}, \tag{6}$$

and it is taken from a uniform distribution between $-1/2$ and $1/2$. The prefactor $\sqrt{24D/(\Delta x)^d \Delta t}$ ensures that the noise has a second moment identical to that of the Gaussian noise integrated over a time interval Δt [18]. Note that the use of a uniform distribution makes no difference and speeds up the computation as it is well accepted [12]. In the operators containing spatial derivatives in Eq. (4) one must now introduce their finite-differences approximations. The Laplacian operator reads

$$\nabla^2 h(\mathbf{x}) = \frac{1}{\Delta x^2}\sum_{\mu=1}^{d}\left[h(\mathbf{x}+\Delta x\hat{e}_\mu,t) + h(\mathbf{x}-\Delta x\hat{e}_\mu,t) - 2h(\mathbf{x},t)\right], \tag{7}$$

where $\hat{e}_\mu$ stands for the basis vector along the μth direction. For the nonlinear term, different possibilities exist that have been argued to lead to different results [15,17]. We restrict ourselves to the two following cases: the standard one,

$$(\nabla h)^2(\mathbf{x}) = \frac{1}{4\Delta x^2}\sum_{\mu=1}^{d}\left[h(\mathbf{x}+\Delta x\hat{e}_\mu,t) - h(\mathbf{x}-\Delta x\hat{e}_\mu,t)\right], \tag{8}$$

henceforth referred to as ST, and the one proposed by Lam and Shin [15], henceforth referred to as LS [19],

$$(\nabla h)^2(\mathbf{x}) = \frac{1}{3\Delta x^2}\sum_{\mu=1}^{d}\{[h(\mathbf{x}+\Delta x\hat{e}_\mu,t) - h(\mathbf{x},t)]^2 + [h(\mathbf{x},t) - h(\mathbf{x}-\Delta x\hat{e}_\mu,t)]^2 + [h(\mathbf{x}+\Delta x\hat{e}_\mu,t) - h(\mathbf{x},t)] \times [h(\mathbf{x},t) - h(\mathbf{x}-\Delta x\hat{e}_\mu,t)]\}. \tag{9}$$

It is worth noting here that the LS discretization does not violate a fluctuation-dissipation theorem that is peculiar of the $(1+1)$ dimensions, unlike the ST discretization [15,17].

B. Pseudospectral discretization

In spectral discretization, the continuum periodic field $h(\mathbf{x},t)$ is first expanded in Fourier modes $\hat{h}_\mathbf{q}(t)$,

$$h(\mathbf{x},t) = \frac{1}{V}\sum_{\mathbf{q}}\hat{h}_\mathbf{q}(t)e^{i\mathbf{q}\cdot\mathbf{x}}, \tag{10}$$

where

$$\hat{h}_\mathbf{q}(t) = \int_V d^d\mathbf{x}\,h(\mathbf{x},t)e^{-i\mathbf{q}\cdot\mathbf{x}}, \tag{11}$$

and $\mathbf{q}\equiv(2\pi n_1/L, \ldots, 2\pi n_d/L)$ is a wave vector defined by d integers n_μ, $\mu=1,\ldots,d$. Similarly, one expands the noise term $\eta(\mathbf{x},t)$ and thereafter applies the Fourier transform to the continuum equation (3). An infinite system of coupled Langevin equations is thus obtained

$$\frac{d\hat{h}_{\mathbf{q}(t)}}{dt} = -\nu\mathbf{q}^2\hat{h}_{\mathbf{q}}(t) - \frac{\lambda}{2V}\sum_{\mathbf{k},\mathbf{k}'}(\mathbf{k}\cdot\mathbf{k}')\hat{h}_{\mathbf{k}}(t)\hat{h}_{\mathbf{k}'}(t)\delta_{\mathbf{k}+\mathbf{k}',\mathbf{q}} + \hat{\eta}_{\mathbf{q}}(t). \tag{12}$$

The Fourier modes $\hat{\eta}_{\mathbf{q}}$ satisfy, according to Eq. (2), the correlation:

$$\langle\hat{\eta}_{\mathbf{q}}(t)\hat{\eta}_{\mathbf{q}'}(t')\rangle = 2VD\delta_{\mathbf{q},-\mathbf{q}'}\delta(t-t'). \tag{13}$$

The spectral discretization then consists in projecting the infinite system (12) on the vector space of periodic functions of period L with only a finite number of nonvanishing Fourier modes. To be more specific, it is assumed that wave vectors $\mathbf{q}$, $\mathbf{k}$, and $\mathbf{k}'$ in Eq. (12) belong to a set $\mathcal{S}$ indexed by integers $|n_\mu|\leqslant N/2$ for $\mu=1,\ldots,d$. In this approximation, the dynamical equations conserve their original form with finite sums replacing the original infinite ones. The noise term and the spatial derivatives are discretized in a similar way. This approach is thus more consistent when compared to finite differences. Furthermore, it provides exact results for the Edward-Wilkinson equation (EW), which can be read off from the KPZ equation (3) with $\lambda=0$. In this case the KPZ equation is reduced to a set of $(N+1)^d$ uncoupled complex Langevin equations. With our method the regularization is performed in Fourier space and its efficiency in reproducing the features of the continuum equation should be compared to that of finite differences at constant number of Langevin equations. Note that the lattice spacing is such that $a=L/N$.

The temporal discretization for the above complex equations is performed by an Euler one time step method [20]. In this case, computation of the linear term as well as the noise is straightforward at each time step. On the other hand, the computation of the nonlinear term

$$\hat{\chi}_q = -\frac{1}{2V}\sum_{\mathbf{k},\mathbf{q}-\mathbf{k}\in\mathcal{S}}[\mathbf{k}\cdot(\mathbf{q}-\mathbf{k})]\hat{h}_{\mathbf{k}}(t)\hat{h}_{\mathbf{q}-\mathbf{k}}(t), \tag{14}$$

which originates from one-half of the square of gradient $\nabla h(\mathbf{x},t)$, necessitates more care. We use a pseudospectral algorithm that hinges on the following four steps.

(a) Extension of the momentum space in such a way so as to have $M+1$ modes $(M>N)$ per direction instead of $N+1$ modes. The supplementary Fourier modes $\hat{h}_{\mathbf{q}}$ are simply set to zero.

(b) Computation, in this extended momentum space, of the spectrum of gradient $\nabla h(\mathbf{x},t)$ by sheer multiplication $\mathbf{q}\hat{h}_{\mathbf{q}}$.

(c) Computation by Fourier transform of $\nabla h(\mathbf{x},t)$ in real space at $(M+1)^d$ collocations points $\mathbf{x}_\mathbf{j}$ located on a d-dimensional hypercubic lattice of elementary size L/M. This is followed by the straightforward calculation of $1/2[\nabla h(\mathbf{x},t)]^2$ at these same collocations points.

(d) By a further Fourier transform of these $(M+1)^d$ values of $1/2[\nabla h(\mathbf{x},t)]^2$, one gets the correct sums $\hat{\chi}_q$ for all wave vectors $\mathbf{q}\in\mathcal{S}$ if M is sufficiently large. The values found for external supplementary Fourier modes are simply discarded.

The entire procedure can be efficiently implemented using a standard Fast-Fourier package [23]. Without a preventive extension of the number of Fourier modes for this specific computation, the exact nonlinear term $\hat{\chi}_q$ would not be obtained for $\mathbf{q}\in\mathcal{S}$: this is the well-known aliasing problem [16,24]. The minimum (and hence most efficient) choice for M turns out to be $3N/2$ [16]. The reasons for this are detailed in Appendix A.

III. SOME RELEVANT QUANTITIES

Kinetically rough surfaces generated by stochastic differential equations such as Eq. (3) generally possess scale invariant properties. We recall below some characteristic quantities in which this behavior becomes manifest as a power law, and define the relevant critical exponents.

The correlation between fluctuations of height between any two points $\mathbf{x}$, $\mathbf{x}+\mathbf{r}$ located at distance r, is given by the height-to-height correlation function

$$G_n(r,t) = \left(\frac{1}{V}\int_V d^d\mathbf{x}\langle|h(\mathbf{x},t)-h(\mathbf{x}+\mathbf{r},t)|^n\rangle\right)^{1/n}, \tag{15}$$

where n is, in general, any real positive number. It is generally assumed that $G_2(r,t)$ has the scaling form

$$G_2(r,t) = r^\chi M\left(\frac{t}{r^z}\right), \tag{16}$$

where the function $M(y)$ is such that

$$M(y)\sim\begin{cases}\text{const}, & y\to\infty,\\ y^\beta, & y\to 0,\end{cases} \tag{17}$$

with $\beta\equiv\chi/z$. z is the dynamical exponent and χ is the roughness exponent. Correlations are then of the form $G_2(r)\sim r^\chi$ in the limit $r\ll t^{1/z}$, whereas they follow the asymptotic limit $G_2(r,t)\sim t^\beta$ for $r\gg t^{1/z}$. In the absence of multiscaling [25,26], the same asymptotic scaling behaviors should be clearly envisaged for different n's. The law (16) can be also connected to the scaling of the roughness $W(t,L)$. This latter quantity, which measures fluctuations amplitudes, is defined as

$$W^2(t,L)\equiv\langle(h-\overline{h_L})^2\rangle, \tag{18}$$

where $\overline{h_L}$ denotes the average height over a volume $V=L^d$. For the Family-Vicsek ansatz [27], such a global scaling reads

$$W(t,L)=L^{\chi}N\left(\frac{t}{L^{z}}\right), \tag{19}$$

where function $N(y)$ is such that $N(y)\to$const when $y\to\infty$ and $N(y)\sim y^{\beta}$ when $y\to 0$. The relation between $W(t,L)$ and $G_2(r,t)$ is discussed in Appendix B. The exponents are similar to those of Ref. (17): quantity β is related to the short time dynamics $W(t,L)\sim t^{\beta}$ and χ to the asymptotic saturation width, $W(t,L)\sim L^{\chi}$. Moreover, note that the roughness may be expressed as (see Appendix C)

$$W^2(t,L)=\frac{1}{V}\sum_{q\neq 0}S(q,t), \tag{20}$$

where $S(q,t)$ denotes the structure factor

$$S(q,t)=\frac{1}{V}\langle\hat{h}_q(t)\hat{h}_{-q}(t)\rangle. \tag{21}$$

In momentum space, one infers the scaling behavior to be (see Appendix C)

$$S(q,t)=q^{-(d+2\chi)}\Phi(q^{z}t), \tag{22}$$

where the function Φ is such that

$$\Phi(q^{z}t)\sim\begin{cases}\text{const} & \text{for } q^{z}t\gg 1,\\ q^{2\chi}t^{2\chi/\beta} & \text{for } q^{z}t\ll 1.\end{cases} \tag{23}$$

Consequently $S(q,t)\sim q^{-(d+2\chi)}$ for large t and $S(q,t)\sim t^{2\beta}$ for small t.

In our simulations we computed the skewness parameter s, which is the (scaled) third moment of the height fluctuations

$$s(t)=\frac{\langle(h-\overline{h}_L)^3\rangle}{\langle(h-\overline{h}_L)^2\rangle^{3/2}}. \tag{24}$$

As observed by Krug *et al.* [28] for $d=1$, this parameter is a good measure of the asymmetry of the distribution of height fluctuations.

Finally, we recall that the KPZ equation carries a close analogy with turbulence theory. For instance, the equivalent of a Reynolds number for the KPZ equation can be defined as [29]

$$\epsilon=\frac{D\lambda^{d}}{\nu^{d+1}}. \tag{25}$$

Moreover, exact heuristic arguments show the existence of the following two length scales:

$$l_{\text{in}}=\left(\frac{\nu^{d+3}}{D\lambda^{d+2}}\right)^{1/2}, \tag{26}$$

$$l_{\text{out}}=\left(\frac{D}{\lambda}\right)^{1/(d+1)}. \tag{27}$$

For a length l smaller than l_{in}, the diffusion linear term is predominant as in the case of viscous scales observed in turbulent flows. Conversely, the nonlinear term is dominant for length $l\gg l_{\text{in}}$, as for the inertial scales in turbulent flows. In fluid dynamics, the outer scale is given by the largest scale available, which is generally provided by the geometry of the specific problem. In the KPZ case [29], it is given by imposing that for scales $l_{\text{in}}\leqslant l\leqslant l_{\text{out}}$, the surface is rough. Note that, since the dimensionless number ϵ is given by

$$\epsilon=\left(\frac{l_{out}}{l_{in}}\right)^{2(d+1)/(d+3)}, \tag{28}$$

there exists an equivalent of the inertial range for large equivalent Reynolds numbers $\epsilon\gg 1$. In this regime, the typical fluctuation of scale l is of amplitude h_l and varies with a typical time t_l given by

$$h_l\equiv l^{2/(d+3)}\left(\frac{D}{\lambda}\right)^{1/(d+3)}, \quad t_l\equiv\frac{l^2}{\lambda h_l}. \tag{29}$$

In the context of the KPZ equation, the inertial range is represented by the strong-coupling regime. This corresponds to $\epsilon\gg 1$. However, the requirement of the existence of a nonnegligible inertial region, that is $l_{\text{out}}\gg l_{\text{in}}$, yields $\epsilon^{f(d)}\gg 1$ with $f(d)=(d+3)/2(d+1)$. Since $f(d)<1$ for $d>1$ then $\epsilon^{f(d)}$ is a slowly increasing function of ϵ. The above remark explains the difficulties of the numerical simulations to reach unambiguous results, due to the long transients that are present in $(2+1)$ and higher dimensions, as we shall further discuss below.

IV. A TEST CASE: (1+1) DIMENSIONS

We compare the performance of the various method in the $(1+1)$-dimensional case. In this instance, the exact value for the steady-state roughness of the continuum equation is known to be [28]

$$W(L)=\sqrt{\frac{D}{12\nu}}L^{1/2}. \tag{30}$$

Such a quantity $W(L)$ has been computed for sizes up to $L=1024$ and parameters $\nu=1$, $\lambda=3$, $D=1$, and averaged over 100 different realizations of the noise and many different steady-state configurations. We have used (a) the finite-differences scheme given by Eq. (8) (ST), (b) the finite-differences scheme given by Eq. (10) (LS), and (c) the pseudospectral scheme (PS). For finite-differences we have set $\Delta x=1$ corresponding to $L=N$ for the pseudospectral method. A first comparison is reported in Fig. 1, where the quantity $\psi(L)=\sqrt{12\nu/DL}W(L)$ is plotted for the three cases. We note that error bars refer to fluctuations within the 100 different noise configurations and that the considered three cases are compared within *identical* statistics.

Unlike the standard discretization, both the pseudospectral and the Lam-Shin discretizations yields exact values for the amplitude (dashed line in Fig. 1), within the error bars. However, the pseudospectral method yields much smaller

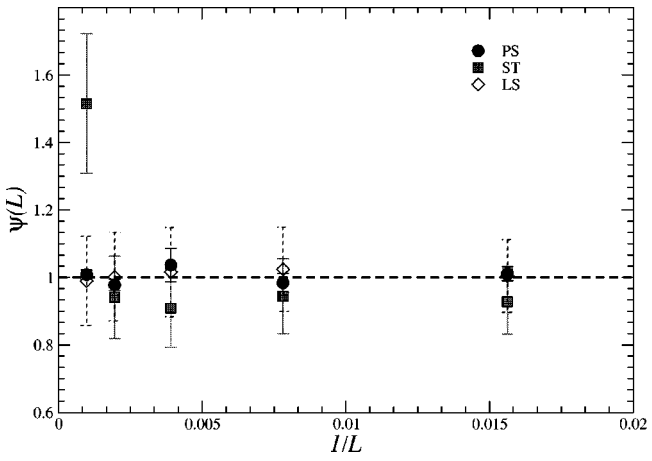

FIG. 1. Quantity $\psi(L) \equiv \sqrt{12\nu/DL}\,W(L)$ in $(1+1)$ dimensions, computed as a function of the size L. $W(L)$ is the steady-state roughness as computed using the standard finite-difference discretization (ST) (with $\Delta x=1$), the Lam-Shin finite-difference discretization (LS) (with $\Delta x=1$), and the pseudospectral discretizations (PS) with $L=N$. All these discretizations have an identical number of degrees of freedom. The number of configurations used in the average is also identical in the three cases. The error bars have been distinguished for clarity: gray line for ST, dashed line for LS, solid line (barely visible) for PS.

fluctuations compared to the Lam-Shin discretization as it can be inferred by comparing the error bars for LS (dashed lines) with those of the PS method (solid line), which are barely visible in Fig. 1 being of the order of the points size.

As a further support to this result, we compute the time evolution of roughness before saturation, which allows to obtain the critical exponent β whose exact value is 1/3. In this case the roughness is averaged over 50 different configurations in all cases. Figure 2 depicts the result. The pseudospectral method follows rather accurately the exact value of the exponent for at least 3 decades, whereas the LS

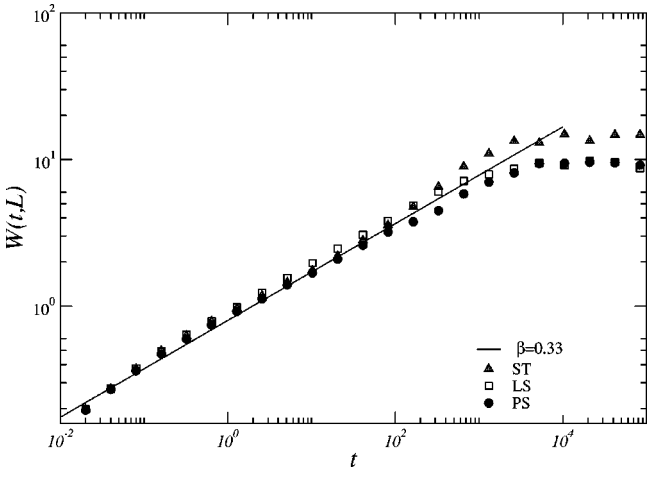

FIG. 2. Roughness $W(t,L)$ in the $(1+1)$-dimensional case as a function of time t for $\lambda=3$. Here the lateral size is $L=1024$, the number of configurations is 50, and ST, LS, and PS stands for standard, Lam-Shin, and pseudospectral discretizations, respectively. The solid line has a slope corresponding to $\beta=0.33$.

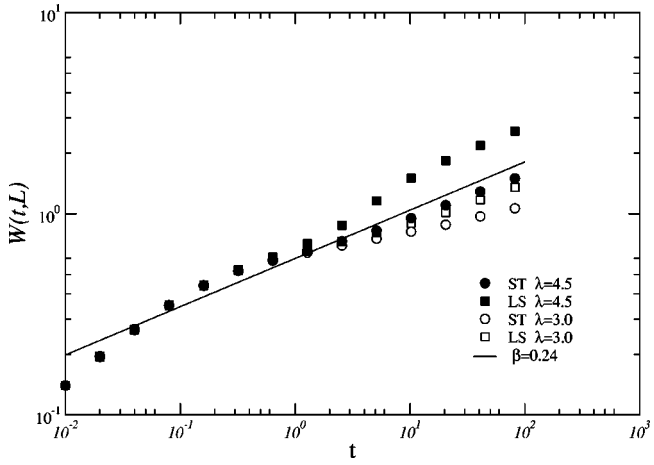

FIG. 3. Roughness $W(t,L)$ obtained from a finite-difference scheme in $(2+1)$ dimensions, as a function of time t for $\lambda=3$,4.5. Here the lateral size is $L=256$, the number of configurations is 50, and ST and LS stands for standard and Lam-Shin discretizations, respectively. The solid line has a slope corresponding to $\beta=0.24$.

method slightly overestimates that value. For the pseudospectral discretization, we have also computed (not shown) the roughness exponent χ with the two different methods illustrated in the next section, always finding an excellent agreement with the exact value $\chi=1/2$.

V. CASE (2+1) DIMENSIONS

Let us consider the most physically relevant case, i.e., that of bidimensional substrate $d=2$. For this purpose, results for various finite differences discretizations and for the pseudospectral discretization are provided for sizes up to $L=256$ and $L=512$, respectively. Computations are averaged over a number of configurations typically of the order of 50–100. The values of ν and D are both set to 1 throughout the rest of this section.

A. Finite difference

To the best of our knowledge, no paper has so far considered a comparison among various finite differences discretizations in dimensions $d=2$. As previously mentioned, we envisage two relevant finite-differences approximations (ST) and (LS) of the KPZ equation. In Fig. 3, a comparison of the roughness $W(t,L)$ as a function of time t is reported for these two methods and two values of the nonlinear parameter ($\lambda=3$ and $\lambda=4.5$). From the figure, one can appreciate the presence of the three regimes (linear regime, KPZ regime, and saturation regime) that are characteristic of any numerical solution of the KPZ equation in $(2+1)$ dimensions when starting from a flat configuration. Both the above values of λ yield a non-negligible region of KPZ regime. From Eq. (25), one has $\epsilon=\lambda^2$ and $\epsilon^{f(d)}=\lambda^{10/6}$, which for $\lambda=3$ give $\epsilon=9$ and $\epsilon^{f(d)}=6.240\ldots$, respectively. For such a moderate nonlinearity ($\lambda=3$) the inertial region is already present, and it increases as λ increases. However, an instability already noticed in previous simulations [12,13] is present for larger

TABLE I. Best estimates of critical exponents β, χ, and z in $d=2$ as reported in the literature. Note that in the numerical solution of the continuum equation we have taken the value of the nonlinear coupling parameters corresponding more closely to the one used in our work. Here KPZ stands for continuum KPZ equation with finite-difference discretization, whereas FT stands for field-theoretical methods. The error bars in the simulations are typically of the order of the last reported digit.

Model	β	χ	z	Reference
RSOS	0.245	0.393	1.607	[11]
RSOS	0.240			[10]
KPZ	0.25	0.39		[12]
KPZ	0.240			[13]
KPZ	0.240	0.404		[14]
Flory	0.25	0.4	1.6	[9,29]
FT	0.25	0.4	1.6	[42]

value of λ. The curvature present in the $\lambda=4.5$ case of Fig. 2, stems from this instability, and it is probably associated with an overestimation of the nonlinearity.

Our results for the critical exponents are in good agreement with previous results reported in the literature for finite-difference schemes. A summary of all these results is provided in Table I for completeness [30].

B. Pseudospectral method

The roughness (20) computed by the pseudospectral method is depicted in Fig. 4 for $L=128$, and various values of λ. It has been computed after averaging over many realizations of noise (typically of the order of $50-100$). The value $\lambda=3$ numerically corresponds to the optimal choice used in previous works [12–14,31,32] in which the strong coupling regime is well displayed (see Fig. 4). The power law for times $t \leqslant L^z$ has been reassessed (see Fig. 5) and

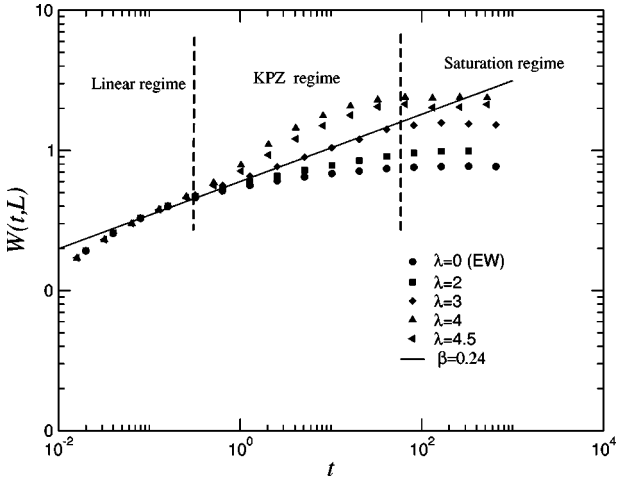

FIG. 4. Roughness $W(t,L)$ as a function of time t for various values of λ as obtained from the pseudospectral methods. Here the lateral size is $L=128$ and the average is over 100 different configurations. We have schematically indicated the typical three regimes found in the simulations.

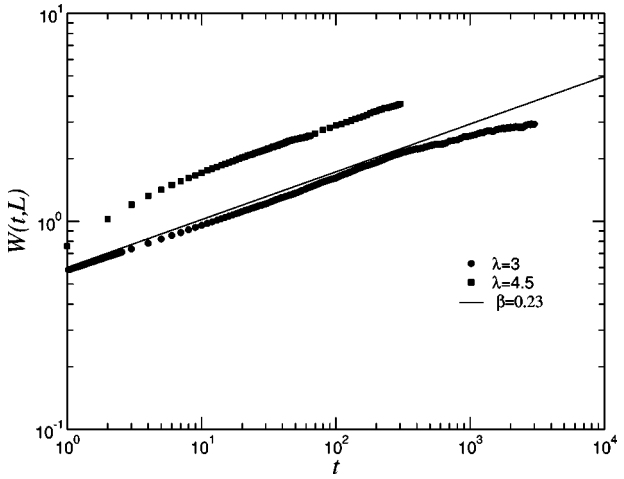

FIG. 5. $W(t,L)$ in $(2+1)$ dimensions, as a function of t when $\lambda=4.5$ and $\lambda=3$. The lateral size is $L=512$ and the number of configurations is 17. The dashed line has a slope corresponding to $\beta=0.23$.

exponent β is evaluated to be $\beta=0.229\pm0.05$ for $\lambda=3$ and 4.5 ($L=512$ is the size used to get this result).

The universal function $N(t/L^z)=W(t/L^z)/L^\chi$ is plotted for $\lambda=3$ in Fig. 6. The exponents z and χ can be estimated using a recent method devised in Ref. [33], which allows the calculation of the two exponents simultaneously with good accuracy. This method provides a more accurate estimate of the roughness exponent χ with respect to the more commonly used procedure of computing the saturation value of W at different system sizes. We obtain $\chi=0.37\pm0.02$ and $z=1.67\pm0.05$.

Two alternative procedures to independently calculate the roughness exponent is based on the computation of the height-height correlation function $G_2(r)$ and of the structure factor $S(q)$ at stationarity. Its results are reported in Figs. 7 and 8. Our best values for the roughness exponent χ are χ

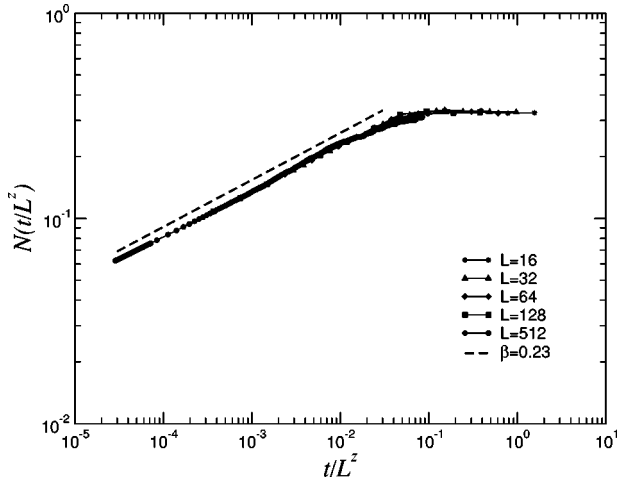

FIG. 6. Collapse plot of the universal function of $N(t/L^z)$ when $\lambda=3$ and various sizes L. The dashed line corresponds to $\beta=0.23$. Parameters are identical to Fig. 4. The obtained values for the exponents are $\chi=0.37\pm0.02$ and $z=1.67\pm0.05$.

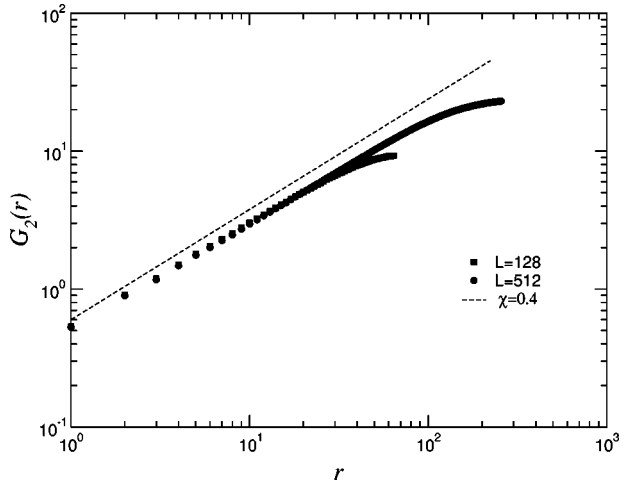

FIG. 7. Height-height correlation function $G_2(r)$ for $\lambda=3$ and sizes $L=128$, 512. The dashed line corresponds to $\chi=0.4$.

$=0.38\pm0.02$ from the correlation function and $\chi=0.40\pm0.01$ from the structure factor. Both these values are, within the error bars, compatible with previous numerical results on the continuum KPZ equation in real space [12–14,31,32] and with recent extensive simulations on RSOS models [11]. As explained in Ref. [34], the computation of the structure factor yields more reliable results of the exponent χ with respect to the commonly used procedure of extracting it from the value of the saturation roughness at various sizes.

Figure 9 depicts the time evolution of skewness $s(t)$ for different sizes L. For $\lambda>0$, the quantity $s(t)$ reaches an asymptotic value (0.25–0.30) indicating a clear-cut asymmetry as opposed to the EW case ($\lambda=0$). This asymmetry in $(2+1)$ is intrinsically different from the one observed for short times both on the Kuramoto-Shivashinsky equation $(1+1)$ [35] and for the single-step one-dimensional model [28], since in that instance the asymptotic value of the skewness should be zero in both cases, due to the Gaussian nature of the probability distribution function. The existence of a

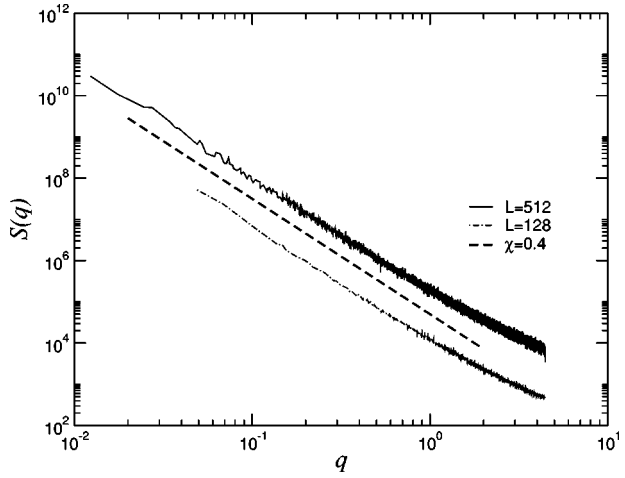

FIG. 8. Structure factor $S(q)$ for $\lambda=3$ and sizes $L=128$, 512. The dashed line corresponds to $\chi=0.4$.

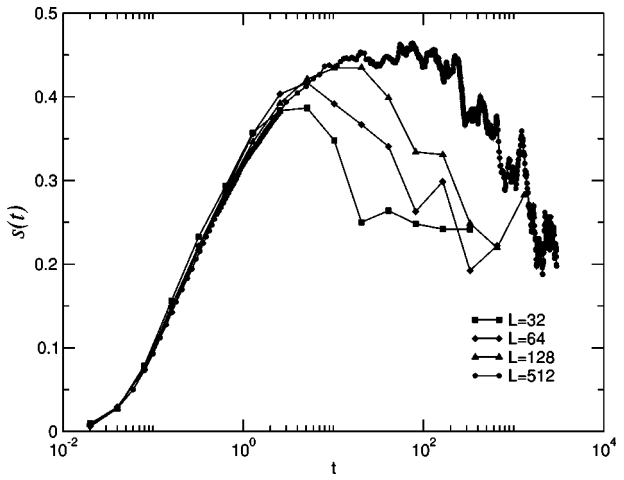

FIG. 9. Skewness $s(t)$ for $\lambda=3$ and sizes L ranging from $L=32$ to $L=512$.

well defined peak for $s(t)$ suggests that this quantity could be a better indicator of the onset of the KPZ regime with respect to the roughness.

It has been suggested [25,26,36], that possible multiscaling behaviors can be inferred by computing the *local* fluctuations $G_n(l,t)$ (where $L/N<l<L/2$, and the extreme case in which l equals the lattice spacing L/N corresponds to the average values of powers of the surface gradient) with respect to time. The reason for this can be traced back to the fine balance between different terms present in the Langevin equation, necessary to get standard scaling. On that basis, one does not expect multiscaling in the KPZ equation case [26]. A direct computation confirms this. First we note that different moments of the stationary state $G_n(r)$ depicted in Fig. 10 have identical scaling. Next we consider the time evolution of $G_n(l,t)$ reported in Fig. 11. This type of calculation has been already performed in Refs. [36] and [25] in the context of discrete models by considering the fluctuations of nearest-neighbors points as a function of time. Here calculations are performed for points located few lattice spac-

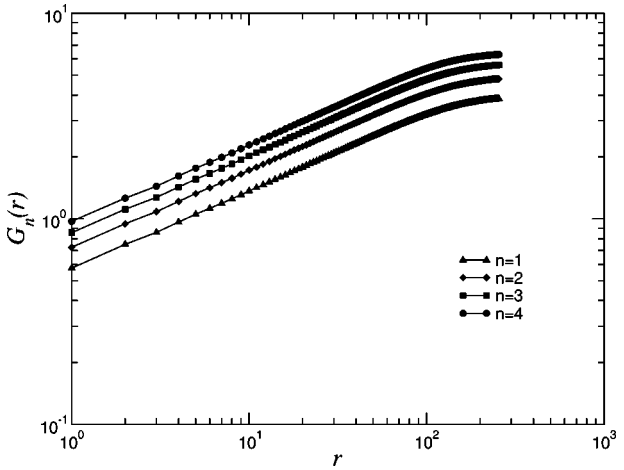

FIG. 10. Various moments of the height difference distribution at stationarity $G_n(r)$ for $\lambda=3$ and size $L=512$. Note that the largest value of r corresponds to $L/2$.

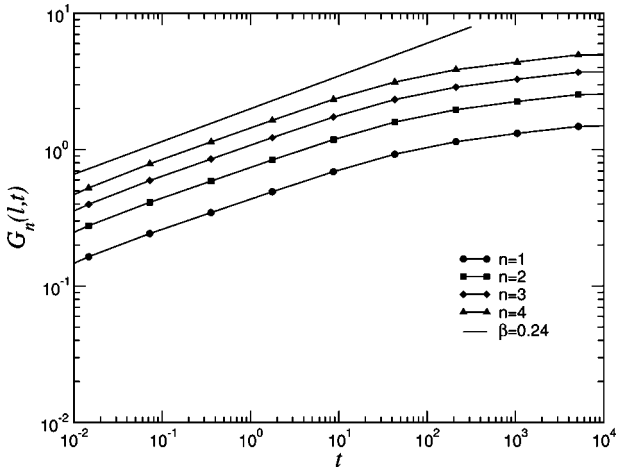

FIG. 11. Various moments of the height-height correlation functions $G_n(l,t)$ for a fixed $l \sim 6L/N$ and $\lambda = 3$, $L = 512$. The solid line corresponds to $\beta = 0.24$.

ings away, i.e., l is included within a circular region $5a \leqslant l \leqslant 8a$ [37]. It is apparent that different moments behave in an equal way in agreement with scaling arguments based on a Flory theory [26].

As a remark, we note that it would be very interesting to compare the above result with an analogous calculation for the Kuramoto-Shivashinsky equation (KS), since there are both analytical [38,39] and numerical [35,40,41] evidences that the (KS) can be mapped, at a coarse grained level, onto a KPZ with a large surface tension coupling ν.

VI. CONCLUSIONS

We have presented a comprehensive study of the pseudospectral method applied to the numerical solution of the KPZ equations. The method can be reckoned as an alternative and highly reliable procedure to the widely exploited finite-difference schemes, and its use in the context of stochastic partial differential equation is new. At the price of a moderate increase in the numerical effort, the method offers an improved accuracy in the computation of the critical exponents, since it does not suffer of the major drawbacks that are common to all the finite-difference schemes in real space. The reason for this is that the functional form of the continuum equation is guaranteed to be maintained, the only approximation made in the calculation being the truncation to a finite rather than infinite number of modes. We have detailed how one can carefully deal with the computation of the nonlinear mode, by using a back and forth transformation between real and momentum space that is more efficient than a brute force computation of the nonlinear term directly in momentum space. We have shown how finite-difference schemes lead to nonnegligible differences in the universal behavior in the temporal region that is accessible to numerical simulations, and explained why the pseudospectral method is the one that both theoretically and practically most closely approaches the continuum limit. As a nontrivial application of the method, we have shown, using extensive simulations and comparing various schemes, that the currently most accepted results for the critical exponents β and χ in $(2+1)$ dimensions, as obtained from RSOS simulations, are directly accessible. We have also presented different ways of computing the roughness exponent χ that yield rather precise and consistent results.

While our results are confined to the KPZ equation in $(1+1)$ and $(2+1)$ dimensions, the method is fully general and can be extended to higher dimensions and other nonlinear continuum equation of the Langevin class.

We believe that the results presented in this work open new perspectives in the computation of the universality classes of nonequilibrium problems by avoiding the uncontrolled use of spatial discretizations from the outset.

ACKNOWLEDGMENTS

Funding for this work was provided by a joint CNR-CNRS exchange program (number 8006), MURST, and INFM. We thank Flavio Seno and Somedra Bhattacharjee for the use of their collapse plot code.

APPENDIX A: THE ALIASING PROBLEM

In this appendix we discuss the necessity of extending the number of Fourier modes to compute the nonlinear terms (14) at each time step, and explain why $M = 3N/2$ is the optimal choice for the size of the extended space. For simplicity, we will treat the $d = 1$ case, the extension to higher dimension being straightforward.

Consider the function $h(x,t)$ at time t. By definition, it contains $N+1$ nonvanishing modes (see Fig. 12)

$$h(x,t) = \frac{1}{L} \sum_{k=-N/2}^{N/2} \hat{h}_{q_k}(t) \; e^{iq_k x}, \tag{A1}$$

with $q_k = 2\pi k/L$. In dimension $d = 1$, one has $\mathcal{S} = \{q_k = 2\pi k/L, N/2 \leqslant k \leqslant N/2\}$ and $V = L$. The computation of the gradient $\partial_x h(x,t)$ or its square at any given point, can be carried out correctly by steps (a)–(c) without any extension of the momentum space. Instead, step (d) is more delicate and it does require the momentum space extension. To understand this point, let us tackle the following more general question. Consider any given periodic function of period L,

$$u(x,t) = \frac{1}{L} \sum_{p=-\infty}^{\infty} \hat{u}_{q_p}(t) e^{iq_p x}. \tag{A2}$$

Assume we want to approximate $u(x,t)$ by a truncated function u^{tr} only containing $2P+1$ nonvanishing modes

$$u^{tr}(x,t) = \frac{1}{L} \sum_{p=-P}^{P} \hat{u}^{tr}_{q_p}(t) e^{iq_p x}. \tag{A3}$$

Since such a function u^{tr} is completely defined if it is known for $M \equiv 2P+1$ points, we choose u^{tr} by imposing that it takes the same values as u on M collocation points $x_j = jL/M \;\; j = 0, \ldots, M-1$. What is the error made on the Fourier modes or, equivalently, how different are $\hat{u}_{q_p}$ and $\hat{u}^{tr}_{q_p}$ for $-N/2 \leqslant p \leqslant N/2$?

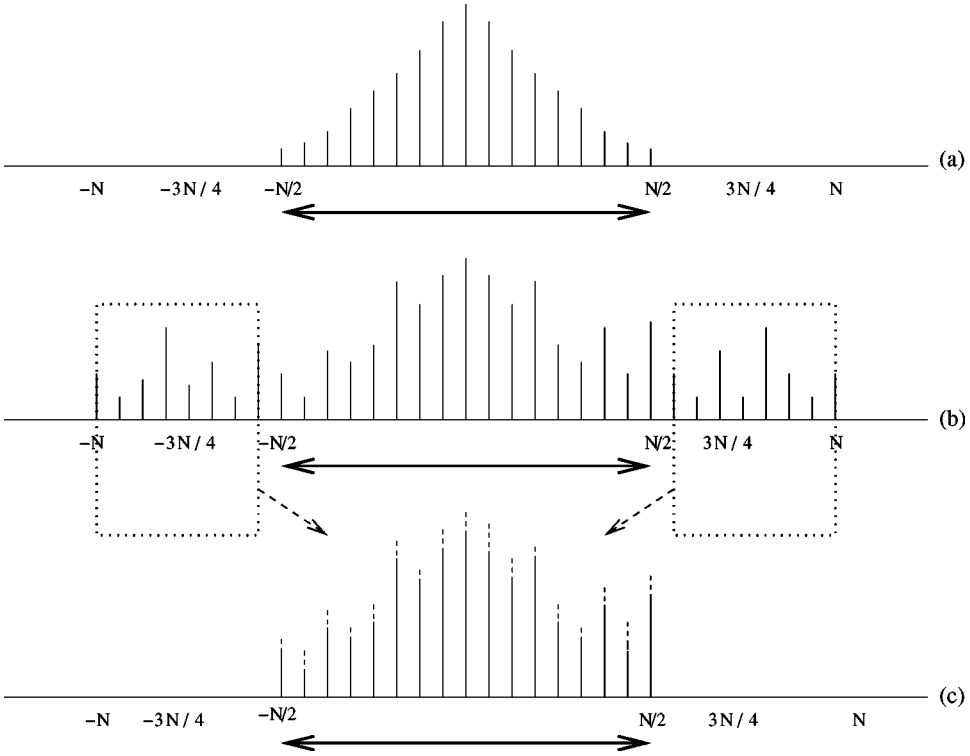

FIG. 12. Illustrating the aliasing problem when $M=N+1$. The arrow line indicates the modes used in the computation. (a) the original field $h(x,t)$; (b) the true function $1/2[\partial_x h(x,t)]^2$; (c) the truncated function associated to $1/2[\partial_x h(x,t)]^2$ when $M=N+1$.

For collocation points $x_j=Lj/M \quad j=0,\ldots,M-1$, the following relation holds:

$$\sum_{p=-\infty}^{\infty} \hat{u}_{q_p}(t)e^{iq_p x_j}=\sum_{p=-P}^{P}\left(\sum_{r=-\infty}^{\infty}\hat{u}_{q_{p+rM}}\right)e^{iq_p x_j}. \quad \text{(A4)}$$

By identification of Eqs. (A3) and (A4), one gets

$$\hat{u}^{tr}_{q_k}(t)=\sum_{r=-\infty}^{\infty}\hat{u}_{q_{k+rM}}, \quad \text{(A5)}$$

for $-P\leqslant k\leqslant P$. Going back to the momentum space, the true spectrum is thus somewhat modified: this is known as the aliasing problem. Note that large wave numbers are, in principle, more affected than small wave numbers.

In the specific case considered, function $u(x,t)$ equals $1/2[\partial_x h(x,t)]^2$ and only contains a finite number of nonvanishing modes: to be precise, the $2N+1$ modes such that $q_k\equiv 2\pi k/L$ with $k=-N,\ldots,N$ (see Figs. 12 and 13). Observe that we are interested only in the modes with $|k|\leqslant N/2$.

If we use for step (d) a truncated function with $M=N+1$ modes ($P=N/2$) to approximate $1/2[\partial_x h(x,t)]^2$, all the Fourier components $\hat{h}_{q_k}$ are modified.

If we use for step (d) a truncated function with $M=2N+1$ modes ($P=N$) to approximate $1/2[\partial_x h(x,t)]^2$, all the nonvanishing Fourier components $\hat{h}_{q_k}$ ($k=-N,\ldots,N$) are correct, even those corresponding to spurious modes $k=-N,\ldots,-N/2-1, \quad k=N/2+1,\ldots,N$. By definition $\hat{h}_{q_{k+rM}}=0$ for $r\neq 0$ hence the infinite sum in Eq. (A5) is reduced to the single term $r=0$.

If we use for step (d) a truncated function with $M=3N/2+1$ modes ($P=3N/4$) to approximate $1/2[\partial_x h(x,t)]^2$, the Fourier modes of the gradient square $q_p=2\pi p/L$ are correctly obtained for $k=-N/2,\ldots,N/2$ and spurious modes $k=-N,\ldots,-N/2-1, \quad k=N/2+1,\ldots,N$ are not but this is of no significance. Again by definition $\hat{h}_{q_{k+rM}}=0$ for $r\neq 0$ and $|k|\leqslant N/2$ hence the infinite sum in Eq. (A5) is reduced to the single term $r=0$ for $|k|\leqslant N/2$. As a consequence the choice $M=3N/2+1$ ($P=3N/4$) for step (d) is the more economical.

APPENDIX B: CORRELATION FUNCTION AND ROUGHNESS

By definition one has

$$G_2^2(r,t)=\frac{1}{V}\int_V d^d\mathbf{x}\langle[h(\mathbf{x}+\mathbf{r},t)-h(\mathbf{x},t)]^2\rangle. \quad \text{(B1)}$$

Expanding this expression and integrating over $\mathbf{r}$ one gets

$$\frac{1}{V}\int_V d^d r G_2^2(r,t)=W^2(t,L)+\frac{1}{V^2}\int_V d^d\mathbf{x}d^d\mathbf{r}\langle h(\mathbf{x},t)h(\mathbf{r},t)\rangle$$
$$+\frac{1}{V^2}\int_V d^d\mathbf{x}d^d\mathbf{r}\langle h^2(\mathbf{x}+\mathbf{r},t)\rangle$$
$$-\frac{2}{V^2}\int_V d^d\mathbf{x}d^d\mathbf{r}\langle h(\mathbf{x}+\mathbf{r},t)h(\mathbf{x},t)\rangle. \quad \text{(B2)}$$

For large V we thus find

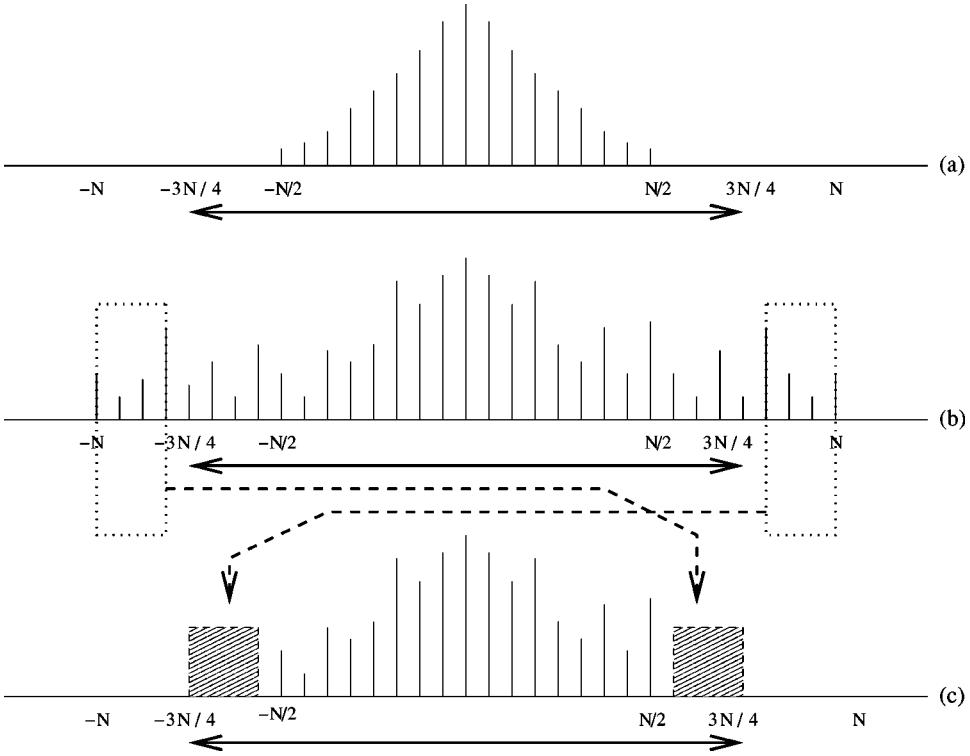

FIG. 13. Solving the aliasing problem with $M=3/2N+1$. The arrow line indicates the considered modes. (a) The original field $h(x,t)$; (b) the true function $1/2[\partial_x h(x,t)]^2$; (c) the truncated function associated to $1/2[\partial_x h(x,t)]^2$ when $M=3/2N+1$.

$$W^2(t,L)=\frac{1}{2V}\int_V d^d\mathbf{r}G_2^2(r,t). \tag{B3}$$

It is then easy to show that if Eq. (16) and Eq. (17) hold true, then the above relation implies that Eq. (19) is valid.

APPENDIX C: SCALING OF THE STATIONARY STRUCTURE FACTOR

Using the Fourier expansion, we get

$$h(\mathbf{x}+\mathbf{r},t)-h(\mathbf{x},t)=\frac{1}{V}\sum_{\mathbf{k}}\hat{h}_{\mathbf{k}}(t)[e^{i\mathbf{k}\cdot(\mathbf{x}+\mathbf{r})}-e^{i\mathbf{k}\cdot\mathbf{x}}]. \tag{C1}$$

By substituting in $G_2^2(r,t)$ one gets after few simple manipulations

$$G_2^2(r,t)=\frac{1}{V^2}\sum_{\mathbf{k}}\langle\hat{h}_{\mathbf{k}}(t)\hat{h}_{-\mathbf{k}}(t)\rangle 2[1-\cos(\mathbf{k}\cdot\mathbf{r})]. \tag{C2}$$

Note that, in the above equation, the term $\mathbf{k}=0$ yields a vanishing contribution to the sum. Eq. (C2) can then be inserted in Eq. (B3), yielding

$$W^2(t,L)=\frac{1}{V^2}\sum_{\mathbf{k}\neq 0}\langle\hat{h}_{\mathbf{k}}(t)\hat{h}_{-\mathbf{k}}(t)\rangle. \tag{C3}$$

Therefore, since we define the structure factor from the relation

$$\langle\hat{h}_{\mathbf{k}_1}(t)\hat{h}_{\mathbf{k}_2}(t)\rangle=V\delta_{\mathbf{k}_1,-\mathbf{k}_2}S(k,t), \tag{C4}$$

we find

$$W^2(t,L)=\frac{1}{V}\sum_{\mathbf{k}\neq 0}S(\mathbf{k},t). \tag{C5}$$

This relation can be checked to be valid directly from the definition of $W^2(t,L)$. On the other hand from Eq. (C2) we also obtain, using Eq. (C4),

$$G_2^2(r,t)=\frac{2}{V}\sum_{\mathbf{k}\neq 0}S(\mathbf{k},t)(1-e^{i\mathbf{k}\cdot\mathbf{r}}) \tag{C6}$$

or inverting

$$\frac{1}{2}\int_V d^d\mathbf{r}G_2^2(r,t)e^{-i\mathbf{k}\cdot\mathbf{r}}=\delta_{\mathbf{k},0}\left(\sum_{\mathbf{k}'}S(\mathbf{k}',t)\right)-S(\mathbf{k},t). \tag{C7}$$

Therefore, for $\mathbf{k}\neq 0$ one gets

$$S(\mathbf{k},t)=-\frac{1}{2}\int_V d^d\mathbf{x}G_2^2(\mathbf{r},t)e^{-i\mathbf{k}\cdot\mathbf{r}}. \tag{C8}$$

If we then assume that

$$G_2^2(r,t)=r^{2\chi}g\left(\frac{t}{r^z}\right), \tag{C9}$$

and using the standard angular integral over the d-dimensional angular variables

$$\int d\Omega_d e^{-ikr\cos(\hat{k}\cdot\hat{r})} = (2\pi)^{d/2}\frac{J_{d/2-1}(kr)}{(kr)^{d/2-1}}, \quad \text{(C10)}$$

one easily gets

$$S(k,t) = k^{(d+2\chi)}\Phi(k^z t), \quad \text{(C11)}$$

where

$$\Phi(k^z t) = -\frac{1}{2}(2\pi)^{d/2}\int_0^{kL} d\lambda\lambda^{2\chi+d/2} g\left(\frac{k^z t}{\lambda^z}\right) J_{d/2-1}(\lambda). \quad \text{(C12)}$$

It is then immediate to see that

$$\Phi(k^z t) \sim \begin{cases} \text{const} & \text{for } k^z t \gg 1, \\ k^{2\chi} t^{2\chi/\beta} & \text{for } k^z t \ll 1. \end{cases} \quad \text{(C13)}$$

[1] A.L. Barabasi and H.E. Stanley, *Fractal Concepts in Surface Growth* (Cambridge University Press, Cambridge, England, 1995).
[2] T. Halpin-Healy and Y.C. Zhang, Phys. Rep. **254**, 215 (1995).
[3] M. Kardar, G. Parisi, and Y.C. Zhang Phys. Rev. Lett. **56**, 889 (1986).
[4] See, e.g., J. Krug, Adv. Phys. **46**, 139 (1997).
[5] E. Frey and U.C. Täuber, Phys. Rev. E **50**, 1024 (1994).
[6] H.K. Janssen, Phys. Rev. Lett. **78**, 1082 (1997).
[7] M. Lässig, Nucl. Phys. B **448**, 559 (1995).
[8] C. Castellano, M. Marsili, and L. Pietronero, Phys. Rev. Lett. **80**, 3527 (1998).
[9] Jin Min Kim and J.M. Kosterlitz, Phys. Rev. Lett. **62**, 2289 (1989).
[10] T. Ala-Nissila and O. Venäläinen, J. Stat. Phys. **76**, 1083 (1994).
[11] E. Marinari, A. Pagnani, and G. Parisi, J. Phys. A **33**, 8181 (2000).
[12] J.G. Amar and F. Family, Phys. Rev. A **41**, 3399 (1990).
[13] K. Moser *et al.*, Physica A **178**, 215 (1991).
[14] M. Beccaria and G. Curci, Phys. Rev. E **50**, 4560 (1994).
[15] C.H. Lam and F.G. Shin, Phys. Rev. E **57**, 6506 (1998).
[16] C. Canuto, M.Y. Hussaini, A. Quarteroni, and T.A. Zang, *Spectral Methods in Fluid Dynamics* (Springer-Verlag, Berlin, 1988).
[17] A. Giacometti and M. Rossi, Phys. Rev. E **63**, 046102 (2001); **62**, 1716 (2000).
[18] H. Risken, *The Fokker-Planck Equation* (Springer-Verlag, Berlin, 1989).
[19] We note a misprint in Eq. (8) of Ref. [17]: $(h_i - h_{i+1})^2$ in the second term should be replaced by $(h_i - h_{i-1})^2$.
[20] As noted in Ref. [21], a more sophisticated procedure using two time steps is not necessarily more efficient for Langevin equations. Indeed we tried some computations with the Heun scheme [22], an analog of the Runge-Kutta method for stochastic equations: it doubles the CPU time without increasing the accuracy.
[21] R. Mannella, in *Noise in Nonlinear Dynamical Systems*, edited by F. Moss and P.V.E. McClintock (Cambridge University Press, Cambridge, 1989).
[22] P.E. Kloeden and E. Platen, *Numerical Solution of Stochastic Differential Equations* (Springer-Verlag, Berlin, 1992).
[23] We have used the FFTW package that is available online at http://www.fftw.org
[24] W. Press, S.A. Teukolsky, and W.T. Vetterling, *Numerical Recipes* (Cambridge University Press, Cambridge, England, 1992).
[25] R. Mohayaee, A.L. Stella, and C. Vanderzande, Phys. Rev. Lett. **87**, 085701 (2001).
[26] J.M. Lopez, Phys. Rev. Lett. **83**, 4594 (1999).
[27] F. Family and T. Vicsek, J. Phys. A **18**, L75 (1990).
[28] J. Krug, P. Meakin, and T. Halpin-Healy, Phys. Rev. A **45**, 638 (1992); K. Sneppen *et al.*, *ibid.* **46**, R7351 (1992).
[29] H.G.E. Hentschel and F. Family, Phys. Rev. Lett. **66**, 1982 (1991).
[30] It is worth noticing that a different finite differences representation of the nonlinear term *effectively* implies a different value of the nonlinear parameter λ, thus making a comparison among different discretizations very difficult.
[31] H. Guo, B. Grossmann, and M. Grant, Phys. Rev. Lett. **64**, 1262 (1990).
[32] A. Chakrabarti and R. Toral, Phys. Rev. B **40**, 11 419 (1989).
[33] S.M. Bhattacharjee and F. Seno, J. Phys. A **34**, 6375 (2001).
[34] M. Siegert, Phys. Rev. E **53**, 3209 (1996).
[35] K. Sneppen, J. Krug, M.H. Jensen, C. Jayaprakash, and T. Bohr, Phys. Rev. A **46**, R7351 (1992).
[36] J. Krug, Phys. Rev. Lett. **72**, 2907 (1994).
[37] Since we are dealing with a continuum equation, any quantity computed at the level of the lattice spacing makes little sense.
[38] V. Yakhot, Phys. Rev. A **24**, 642 (1981).
[39] C. Jayaprakash, F. Hayot, and R. Pandit, Phys. Rev. Lett. **71**, 12 (1993).
[40] S. Zaleski, Physica D **34**, 427 (1989).
[41] B.M. Boghosian, C.C. Chow, and T. Hwa, Phys. Rev. Lett. **83**, 5262 (1999).
[42] M. Lässig, Phys. Rev. Lett. **80**, 2366 (1998).